Comm. in Asteroseismology
Vol. 156, 2008

Data Reduction pipeline for MOST Guide Stars and Application to two Observing Runs

M. Hareter[1], P. Reegen[1], R. Kuschnig[1], W. W. Weiss[1], J. M. Matthews[2], S. M. Rucinski[3], D. B. Guenther[4], A. F. J. Moffat[5], D. Sasselov[6], G. A. H. Walker[2]

[1] Institut für Astronomie, Türkenschanzstrasse 17, A-1180 Vienna, Austria
[2] Department of Physics & Astronomy, University of British Columbia, 6224 Agricultural Road, Vancouver, B.C., V6T 1Z1, Canada
[3] Department of Astronomy, University of Toronto, 50 St.George Street, Toronto, Ontario, M5S 3H4, Canada
[4] Department of Astronomy and Physics, St. Mary's University, Halifax, Nova Scotia, NS B3H 3C3, Canada
[5] Département de physique, Université de Montréal, Montréal, Québec, QC H3C 3J7, Canada
[6] Harvard-Smithsonian Center for Astrophysics, Cambridge, Massachusetts, MA 02138, USA

Abstract

A Data Reduction pipeline for MOST[1] Guide Star data is presented together with the results obtained for two observing runs in 2004 (i.e. κ^1 Ceti 2004 and HR 1217 2004 runs) containing four and seven Guide Stars respectively. Among these Guide Stars, four are clearly variable with only one known before the MOST observations: the long period variable HD 24338 (M2III). The data reduction relies on the decorrelation technique employed by Reegen et al. (2006) for their data reduction pipeline of MOST Fabry targets. The main difference is that the MOST Guide Star data include no background information. A coarse on-board background subtraction is performed, but leaves considerable residual stray light in the data, which is subject to a more sophisticated reduction

[1]Based on data from the MOST (Microvariability & Oscillation of STars) satellite, a Canadian Space Agency mission jointly operated by Dynacon, Inc., the University of Toronto Institute of Aerospace Studies, and the University of British Columbia, with assistance from the University of Vienna, Austria.

technique. Since at least four stars are observed simultaneously, common features of the light curves can be recognized and removed. Among different data reduction methods, the decorrelation technique is more versatile and often has better results than differential photometry or data smoothing.

Individual Objects: HD 20884, HD 20790, HD 24338, HD 24217

Introduction

MOST (Microvariability and Oscillations of STars) is a Canadian microsatellite space mission, which carries a 15-cm Rumak-Maksutov telescope. For a full description before and after launch see Walker et al. (2003) and Matthews (2004). Three different photometric modes are available simultaneously:

(a) Fabry imaging: the telescope entrance pupil is imaged as an annulus of 40 pixels diameter, enhancing the total signal and reducing the influence of satellite jitter. Reegen et al. (2006) developed a reduction pipeline for data obtained in this mode, resolving linear correlations between target and background pixels.

(b) Direct imaging: stars are imaged directly, i.e. the light does not pass through one of the Fabry lenses. For this mode, 20×20 pixel subrasters are used and the images are stored as extentions in the FITS headers. Rowe et al. (2006) and Huber & Reegen (2008) developed direct imaging data reduction pipelines independently, the latter relying on the decorrelation technique.

(c) Guide Star photometry: this mode of photometry was originally intended for guiding only, but the data quality is sufficiently high to be used for science. A data reduction pipeline for this mode is presented here. In early 2006 the MOST Guiding CCD, which was used for gathering the Guide Star data, failed due to a charged particle hit. Since this event the Science CCD took over its function. Originally, the reduction method presented here was developed for the Guiding CCD. Since the data format did not change, it is fully applicable for Guide Star data from the Science CCD.

MOST light curves suffer from stray light from the bright Earth. A periodic non-sinusoidal modulation of the light curves is present in any observed data set. A detailed study of the sources of stray light and other instrumental effects can be found in Reegen et al (2006). To mitigate the stray light and other instrumental signal, the decorrelation method was employed for the Guide Star data.

The data reduction routine consists of two IDL-based programs, one for data extraction and one for the data reduction. The frequency analysis was done using SigSpec (Reegen 2007). Meanwhile more than 1000 stars have been observed. In this paper, we denote Guide Stars by the lower case letter g followed by a number. For the sake of convenience, we modify the Julian Date (JD) to JDM = JD - 2 451 545 (epoch 2000.0). In the follwing sections, the data format of MOST observations is described, three approaches for data reduction are discussed and the results of two runs using the decorrelation technique are described.

Data Format and On-board Background Subtraction

MOST has two Science Data Stream (SDS) formats: one contains compressed images of the primary science target (SDS1) and one contains a 2×2 pixel binned image (SDS2). Both SDS formats contain information on the Guide Stars within the FITS headers. One FITS file usually contains one exposure of the Fabry image, the direct images (20×20 pixel subrasters) as extensions and the Guide Star data as header entries. No Guide Star images are available and the only information available is the intensity and the integration time, as shown by the following example:

```
...
 JD_OBS       1748.2233094  / Julian Date - 2,451,545
 NUM_GS       4             / Number of guide stars
 GS_I0000     144114        / Intensity of guide star number 0
 GS_T0000     26500         / Integration time for guide star in milliseconds
 GS_I0001     35430         / Intensity of guide star number 1
 GS_T0001     26500         / Integration time for guide star no. 1
 ...
```

In later FITS header versions, the Heliocentric Julian Date was implemented and labeled JD_HEL. At least four Guide Stars must be observed simultaneously for pointing requirements. Due to the limited downlink capacity of MOST, the Guide Star information is processed and compressed on board the satellite. For each Guide Star, a 20×20 pixel (or $1' \times 1'$) raster is used. Short exposure times are required due to pointing requirements, hence image stacking is used. Individual frames to be stacked are hereafter referred to as subexposures. The integration time of a subexposure is typically between 0.3 and 3.0 seconds. The smaller the integration time, the higher the sampling rate and the better the pointing. On the other hand, the longer the integration time, the better the photometric precision.

The background is determined as the mean value of the first and the last row of the individual subraster. This mean value is referred to as threshold. Inten-

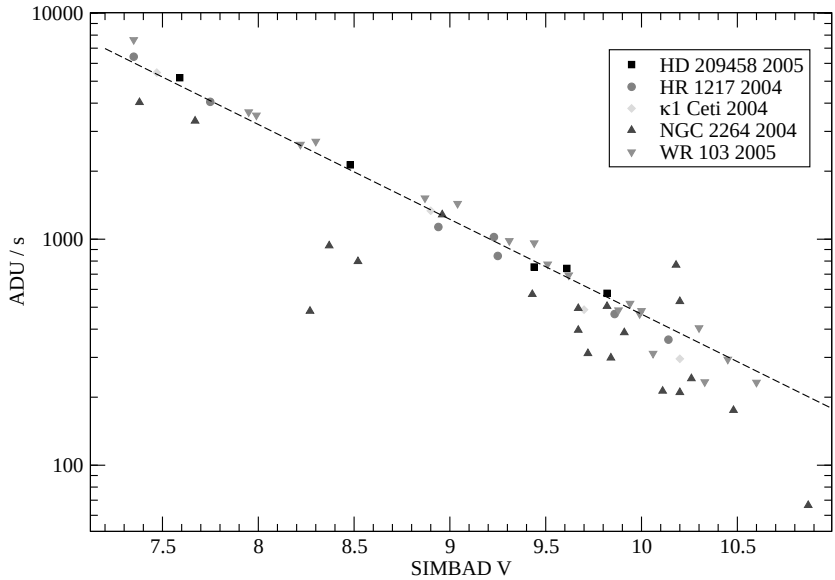

Figure 1: V magnitude versus count rate (ADU/s). Guide Star data of five observing runs are shown. The dashed line corresponds to the expected count rate for a given magnitude.

sities exceeding the threshold are considered stellar signal. Only the intensities of these pixels are summed up, subtracting the individual threshold from each subexposure. This corresponds to an aperture photometry, where the aperture is determined dynamically. The intensity of a stacked exposure (e.g GS_I0000 listed above) is obtained by summing up the intensities of all subexposures. Since fainter stars have fewer illuminated pixels, this kind of aperture photometry produces systematically lower intensities for fainter stars than expected, which is illustrated in Fig. 1. Mean ADU values for individual stars are plotted vs V magnitude according to SIMBAD. Since MOST has a custom broadband filter, those values are not exactly comparable, but to a sufficient accuracy for our purpose. The dashed line corresponds to the expected ADU value for a Guide Star with given magnitude m_V. Fainter stars are systematically below the line.

Unfortunately, the threshold is not stored in the FITS header. Hence no information on the background is available. This limits the precision of the Guide Star photometry, but still the data are of high quality and time coverage.

Data reduction Techniques

Decorrelation

For data reduction, we used the approach developed for science targets observed in Fabry Imaging mode (Reegen et al. 2006). This method resolves linear correlations between the intensities of target pixels and those of background pixels. Since no background information is available for Guide Stars, the light curves of non-variable Guide Stars are used instead. The observed light curves of the Guide Stars are classified as variables and non-variables by a quick-look analysis. Correlation coefficients between a particular variable star's light curve and all non-variable light curves are calculated.

Subsequently, the comparison light curves are sorted by descending correlation coefficients. Then the linear regressions of the variable star's light curve in relation to the light curves of comparison stars are subtracted from the variable's intensities. The rank of correlation coefficients determines the order in which non-variable light curves are picked. All light curves are decorrelated vs. the light curves of all reference stars according to their ranking.

The number of decorrelations is the number of constant reference stars in the sample. Resolving linear correlations between light curves mitigates all Fourier amplitudes of a variable star rather than only the unwanted ones. In the case of Guide Star photometry, the amount of decorrelations performed is small enough to neglect this issue.

Fig. 2 represents the intensity vs intensity plot of the two light curves of non-variable Guide Stars g6 and g1 and the linear regression which is subtracted subsequently. Correcting for linear regression causes common signal (e.g. orbital variations) to be mitigated. Since the pattern (see Fig. 2) is generally more complicated than the linear approximation (Fig. 9 in Reegen et al. 2006), stepwise multiple linear regression is employed: different CCD positions are exposed to different stray light conditions, and correcting for more than one reference star permits to cover a greater variety of contamination patterns.

Fig. 3 shows the effect of decorrelation in a sample with many constant reference stars. The periodic modulation at the MOST orbit frequency at $14.19\,\mathrm{d}^{-1}$ is reduced by a factor of about 10. The presented part of the light curve corresponds to a δ Scuti star observed by MOST simultaneously with Procyon in 2007. The peaks near $25\,\mathrm{d}^{-1}$ indicate intrinsic signal, which is practically not affected by the decorrelation method. This reduction of instrumental signal is not due to outlier rejection, because the term "raw data" is used here in the sense of outlier corrected data before decorrelation.

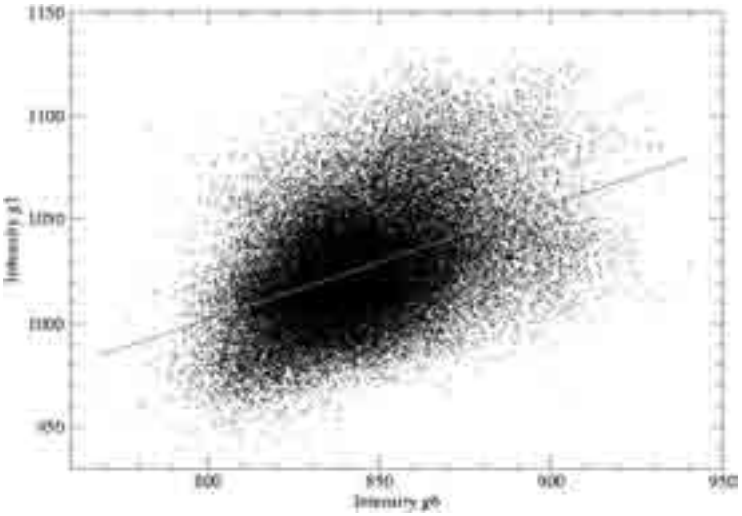

Figure 2: Intensity vs. intensity plot of two Guide Stars of the HR 1217 2004 run. The solid line shows the linear regression.

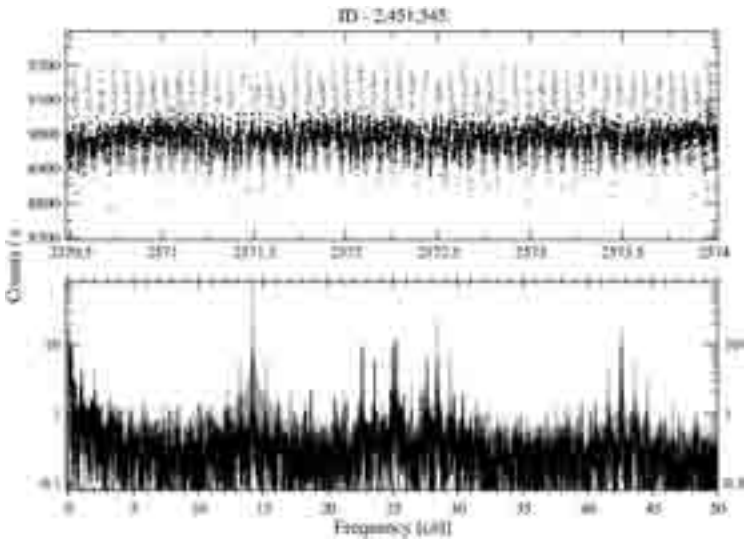

Figure 3: Unprocessed data (gray) compared to decorrelated data (black). In this particular observing run 12 non-variable Guide Stars were available. The decorrelation technique significantly reduced the residual power near the MOST orbit frequency (14.19 d^{-1}) and near its harmonics. The scale on the y-axis is logarithmic for better visibility.

Limitations

There are a few limitations to the decorrelation method. When applied to MOST Fabry data, the background pixels are well-defined and isolated from the stellar signal. The MOST Guide Star photometry does not provide independent information in the form of background pixels on the CCD, hence presumably constant reference stars must be used instead. The correlation of background pixels to target pixels is generally better than the correlation between stellar light curves.

The decorrelation method cannot identify a variable star independently. Using a variable as a reference introduces spurious signal into all the stars in the sample; thus, a variable may not be discovered. Fig. 4 shows the effect of the decorrelation technique, if a variable reference star is used accidentally. The intrinsic signal of g1 is introduced into all other constant reference stars (g2 vs. g1 is shown as an example). Comparing the resulting frequencies after a SigSpec analysis of the individual stars, the pulsation signal of g1 may be misinterpreted as common instrumental periodicities.

A further issue is that if the stray light is extremely high or if the targets have been observed only during orbital phases of maximum stray light (for example switch targets), the decorrelation method significantly increases the time domain point-to-point scatter. For those targets, the decorrelation technique may not be an appropriate approach.

If the stray light distribution is extremely inhomogeneous on the CCD, Guide Stars show very different light curves. In this case, Guide Stars close to the variable should be used rather than stars showing very different stray light behavior.

Due to the rejection of outliers, the spectral window may become worse. Outliers produced at random and uniformly distributed in time will not affect the spectral window, but cosmic ray impacts occur more frequently during South Atlantic Anomaly passages of the spacecraft, and their rejection will introduce aliasing at the orbital frequency of the satellite. However, these peaks will show up in the spectral window and are easy to identify also in the Fourier spectrum of a light curve.

Other Approaches

Differential Photometry

The three-star differential photometry may be also applied to MOST Guide stars. However, the comparison stars have to be selected carefully for two reasons: Obviously, they may be variable and the stray light behavior may be very different at different CCD positions. Stray light may also move across the

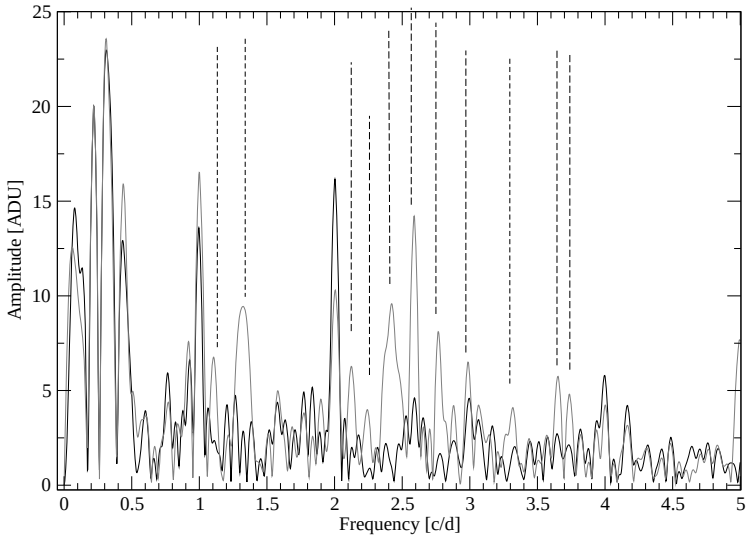

Figure 4: Fourier amplitude spectra for Guide Star g2 before (solid black line) and after (solid gray line) decorrelation vs. g1. The dashed lines mark the frequencies intrinsic to g1 which were transferred to g2 by the decorrelation.

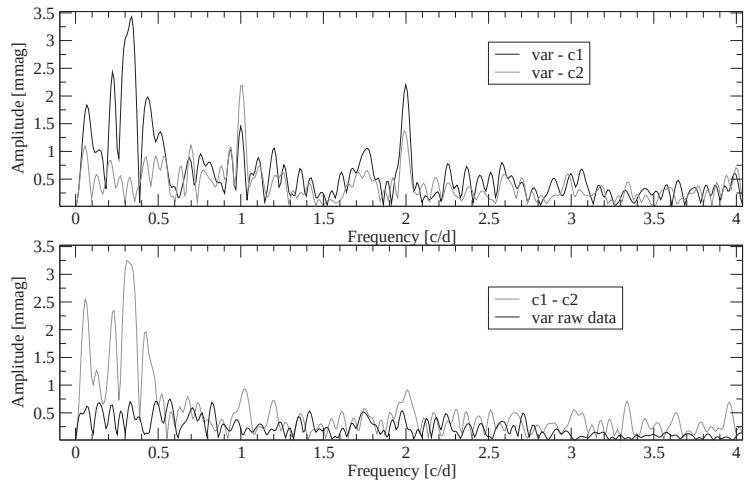

Figure 5: Application of the three star photometry to the data of the bright star g0. Top panel shows var - c1 and var - c2, bottom panel shows c1 - c2 and the Fourier spectrum of the unprocessed data. The peaks at $0.3\,\mathrm{d}^{-1}$ may be due to intrinsic variablity of c1.

CCD, which means that stray light influences light curves of stars at different positions at different times. This effect complicates the differential photometry. In many cases, there are no appropriate comparison stars available. For example in the κ^1 Ceti 2004 run the two stars which are classified as non-variable are too faint. Fig. 4 shows the application of the three star photometry to the data of g0 (var) in the κ^1 Ceti 2004 run, where the two faint stars are used as comparison stars (c1 and c2). The pulsation signal of the bright K giant is lost in the noise introduced by the faint comparison stars. In this run, the differential photometry cannot be applied.

Another approach may be to calculate a mean light curve of the constant stars and subtract this averaged light curve from the variable star data. The problems mentioned above have to be taken into account also in this case.

Data Smoothing using Periodic Filter Functions

In the time domain, filtering may be considered the convolution of a response function $\rho(\tau)$ and the observable $x(t)$,

$$x_F(t) = \rho * x = \int_{-\infty}^{\infty} d\tau\ \rho(\tau)\, x(t+\tau)\ . \tag{1}$$

The filtered observable is then $x - x_F$.

The Fourier transform $\widetilde{x_F}$ is given by the product of the transformed response function, $\tilde{\rho}$, and the transformed observable, $\tilde{x}$, according to

$$\widetilde{x_F}(\omega) = \tilde{\rho}(\omega)\, \tilde{x}(\omega)\ . \tag{2}$$

For convenience, we use the *transformed filter function* (TFF)

$$\Psi(\omega) = 1 - \tilde{\rho}(\omega) \tag{3}$$

rather than the transformed response function $\tilde{\rho}(\omega)$.

The most elementary application of a periodic filter in order to correct for unwanted periodicities in time series data is a set of equidistant rectangular profiles of width δ. The distance of consecutive profiles in time shall be denoted Δ. In the present case, Δ is equal to the orbital period of MOST. Furthermore, we note that due to symmetry, the number of such rectangular profiles will always be odd, say $2N+1$. The number of rectangles determines the *time bandwidth* of the filter, whereas the orbital phase interval mitigated by the filter shall be called the *phase bandwidth* and is adjusted by δ. Given these specifications, the TFF evaluates to

$$\Psi(\omega) = 1 - \left| \frac{2}{(2N+1)\,\omega\delta} \left(\sin\omega\frac{\delta}{2} + 2\sum_{n=1}^{N} \cos n\omega\Delta\ \sin\omega\frac{\delta}{2} \right) \right| . \tag{4}$$

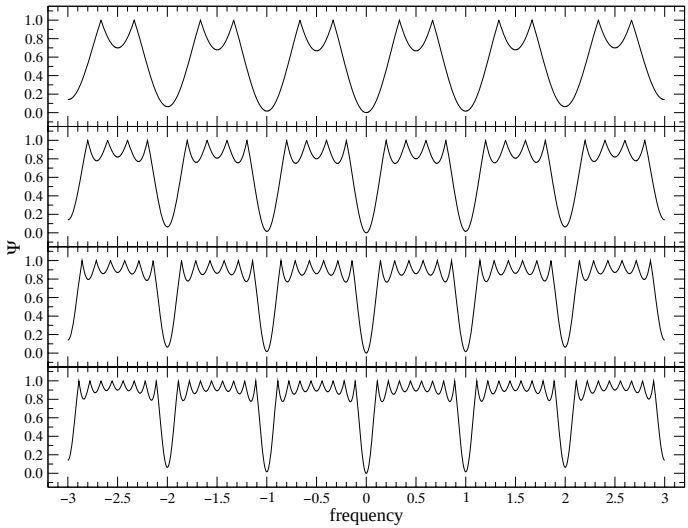

Figure 6: TFFs of periodc rectangular time-domain filters for 3, 5, 7, and 9 rectangles (*top* to *bottom*), i. e., $N = 1$, 2, 3, and 4, respectively. All panels refer to $\Delta = 1$, $\delta = 0.1$.

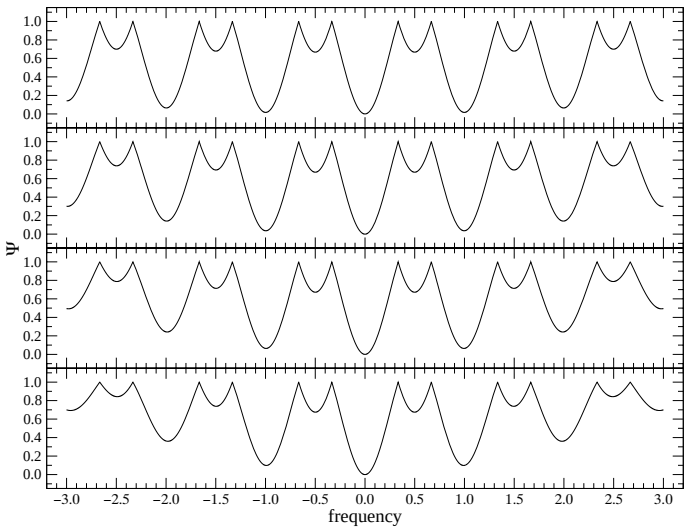

Figure 7: TFFs of periodc rectangular time-domain filters for phase bandwidths $\delta = 0.1$, 0.15, 0.2, and 0.25 (*top* to *bottom*). All panels refer to three rectangular profiles (i. e., $N = 1$) with $\Delta = 1$.

Figs. 6, 6 display the TFFs for different values of N and δ, respectively. Setting $\Delta = 1$ provides the frequency to be in units of orbital frequency. Thus, peaks reaching zero or values close to zero in the Figures refer to the vicinity of the orbital frequency of the spacecraft (and harmonics) and illustrate the efficiency of the filter. On the other hand, there are also periodicities in between these major peaks, which are unwanted, because they introduce systematic over- and under-estimation of selected frequency regions. This is a principal and serious disadvantage of periodic time-domain filters, which can be overcome by more sophisticated approaches only to a limited extent.

Fig. 6 illustrates the influence of the time bandwidth on the TFF: the TFFs for 3, 5, 7, and 9 rectangular profiles ($N = 1$, 2, 3, and 4, correspondingly) are displayed, all for a phase bandwidth $\delta = 0.1$. Employing more rectangular profiles (i. e. increasing the time bandwidth) narrows the major peaks of the TFF around the orbital frequency and its harmonics and increases the number of minor peaks in between. The amplitude of these minor peaks is also slightly reduced.

Fig. 6 contains four panels associated to the TFFs for phase bandwidths $\delta = 0.1$, 0.15, 0.2, and 0.25, all for three rectangular profiles (i. e., $N = 1$). The phase bandwidth δ influences the effect of the filter on orbit harmonics: narrow-phase-band filters are more efficient in this respect.

However, the problem that periodic time-domain filters affect the entire frequency range and consequently also stellar signal rather than only instrumental pseudo-periodicities, persists independently of the parameter settings. As an example, the light curve of HD 20790 (Guide Star g1 of κ^1 Cet) is filtered with $\Delta = 101.4$ min, $N = 5$, and $\delta = 0.1$. Fig. displays the DFT amplitude spectra of the two light curves (raw and filtered) in the top panel. The filtered spectrum (gray curve) shows the mitigated orbit-related peaks, but their $1\,\mathrm{d}^{-1}$ sidelobes, which represent modulations in the stray light contamination, remain practically unaffected. The bottom panel contains the TFF, as obtained from the amplitude spectra and clearly visualizes the effect of systematic over- and under-estimation of selected frequency regions. Unfortunately, the peak amplitudes around $1\,\mathrm{d}^{-1}$, which are of particular interest for γ Dor variables, are massively distorted.

Application to two Fields and Results

Analysis of the Guide Stars of the κ^1 Ceti 2004 Observing Run

The final reduction of the Guide Stars was performed using the decorrelation method described above. Table 1 gives the observation details of both runs. The stray light conditions in these observations were optimal, hence the raw data are of extraordinary quality compared to many other runs. Fig. 9 compares the raw data to the 3-σ clipped data and the reduced data of g1 as an

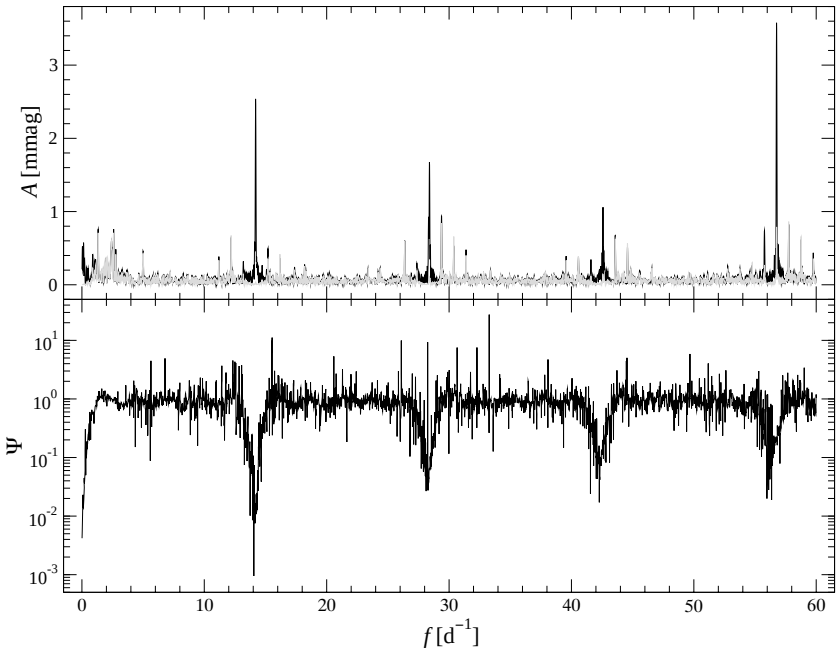

Figure 8: *Top:* Amplitude spectra of the HD 20790 Guide Star photometry. The *black* curve refers to the raw data, the *gray* curve to the light curve after application of a periodic rectangular time-domain filter with $\Delta = 101.4$ min, $N = 5$, and $\delta = 0.1$. *Bottom:* TFF derived from the amplitude spectra in the top panel.

example. The spectral window before and after processing the data are shown in Fig. 10, Fig. 11 shows the Fourier spectra of g1. The gray color refers to the 3-σ clipped data, and the Fourier spectrum of the decorrelated data is represented by the black graph. The sidelobes of the MOST orbit frequency and its harmonics are mitigated by decorrelation. However, the orbit peak at 14.19 d^{-1} is increased significantly from 2.4 mmag in the raw data to 3.1 mmag in the decorrelated data. The first harmonic at 28.38 d^{-1} increases slightly, whereas higher overtones are damped.

This observing run contains two variables and two rather faint comparison stars, where one (g2) might also be a long period variable, because the Fourier spectrum contains a power excess in the lowest frequency regime. Despite this fact, this star was also used for the decorrelation technique, which affects only the frequency region below 0.5 d^{-1}. Power in this frequency region has been ignored. The variables are considerably brighter than the two comparison stars, hence the decorrelation technique does not decrease the instrumental

Run	κ^1 Ceti	HR 1217 run
Date of the observations (2004)	Oct 15 to Nov 4	Nov 5 to Dec 4
Length of final dataset [d]	19.63	29.02
Integration time [s]	26.25	26.4
Sampling time [s]	35	35
# of raw data-points	48 869	70 066
# of data-points after reduction	44 357	64 698

Table 1: Details of the MOST photometry of the κ^1 Ceti 2004 and HR 1217 runs

ID	GSC-ID	HD / BD	SpT.	V [mag]	parallax [mas]
g0	00060-00509	HD 20884	K2III	7.47	5.76 $\pm$0.57
g1	00060-01499	HD 20790	F4IV	8.9	6.70 $\pm$0.86
g2	00060-00969	-	F8	10.2	-
g3	00060-00845	BD +03 459	K2III	9.7	-

Table 2: Information on the κ^1 Ceti Guide Stars including the new HIPPARCOS parallaxes (van Leeuwen 2007).

ID	Standard deviation [mmag]	Point-to-point scatter [mmag]
g0 raw	5.754	3.130
g0 reduced	5.582	3.000
g1 raw	9.740	8.145
g1 reduced	7.601	6.472

Table 3: Improvement in terms of standard deviation and point-to-point scatter of the two variable stars among the κ^1 Ceti Guide Stars by decorrelation.

artifacts significantly. However, the RMS deviation of the data sets, which are important for the frequency analysis, were decreased: for g0 only 3% reduction was achieved, for g1 22%. The results of the frequency analysis using SigSpec were compared for the four light curves. Only frequencies that are unique for the data sets, within the frequency error of ± 0.013 d^{-1} or $1/(4T)$, where T denotes the length of the dataset, were accepted for each star (Kallinger et al. 2008b).

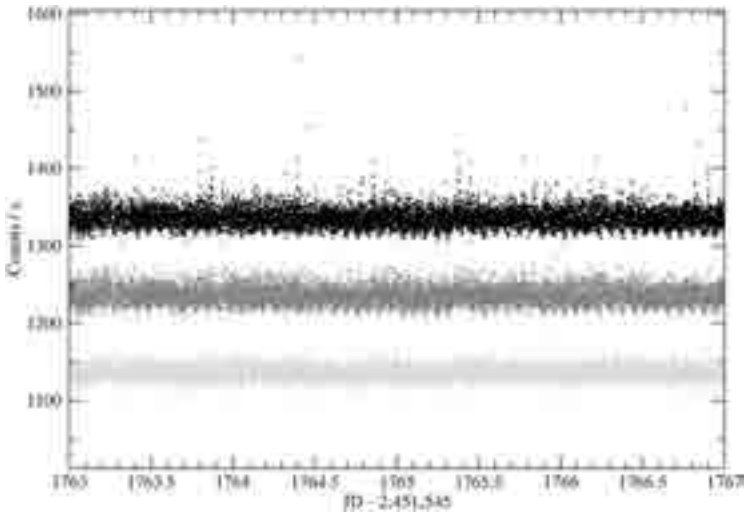

Figure 9: Comparison of the g1 light curves: raw data (top), 3-σ clipped raw light curve (middle) and decorrelated data (bottom). A subsample of four days is shown with vertical offset for the three graphs, for better visibility.

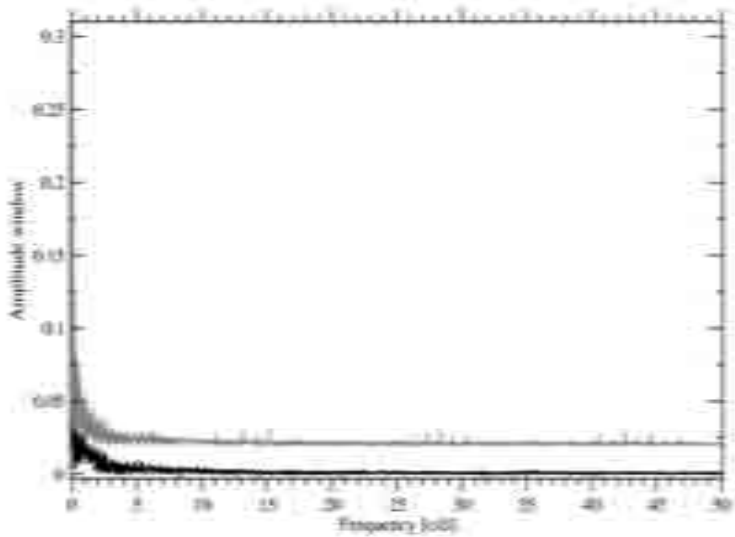

Figure 10: Comparison of the spectral windows for the raw data (black line) and the processed data (gray line, offset 0.02 for visibility). The spectral window changes marginally due to periodic rejection of outliers, hence aliasing plays a minor role.

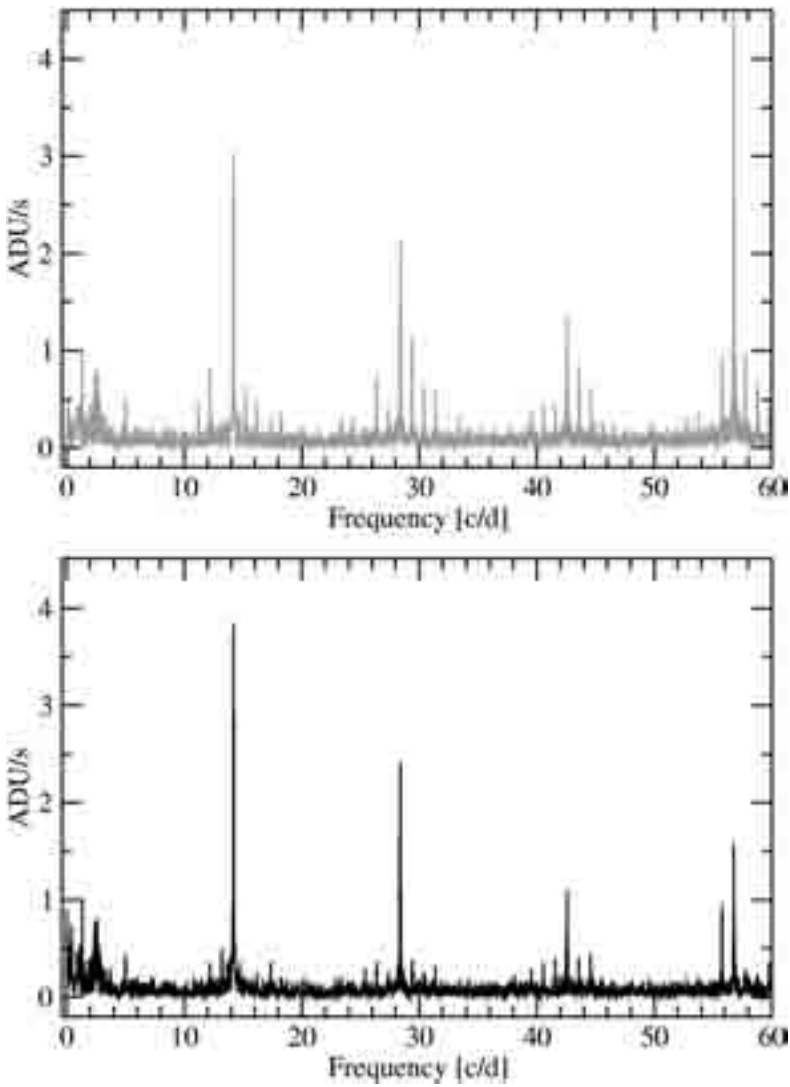

Figure 11: Comparison of the Fourier spectra of 3-σ clipped data (upper panel) and decorrelated data (bottom panel). The sidelobes of the MOST orbit frequency and also the higher order harmonics are reduced.

Results of the Guide Stars of the κ^1 Ceti 2004 Observing Run

The red giant HD 20884

The final light curves for both stars are shown in Fig. 12 and the Fourier spectrum in the range from 0 to 6 d^{-1} is displayed in Fig. 13. Kallinger et al. (2008a) found evidence for radial and nonradial pulsations in this red giant and drew conclusions concerning the mode lifetime. The authors also state that the model which fits the frequencies best is too luminous compared to the HIPPARCOS parallax published in 1997 (ESA 1997).

The new reduction of the HIPPARCOS data was published by van Leeuwen (2007) and the new parallax puts the star at a larger distance. Hence, the star is more luminous. The absolute magnitude M_V was estimated employing $m_V - M_V = 5 \log r - 5$, where r is the distance in pc. The luminosity is estimated using $L/L_\odot = 79.43 \times 10^{(-0.4(M_V+BC))}$ (Kallinger et al. 2008a). Taking the parallax error and the bolometric correction into account, the bolometric luminosity of HD 20884 is estimated between 40 and 60 $L_\odot$ which is still consistent with the value found by those authors.

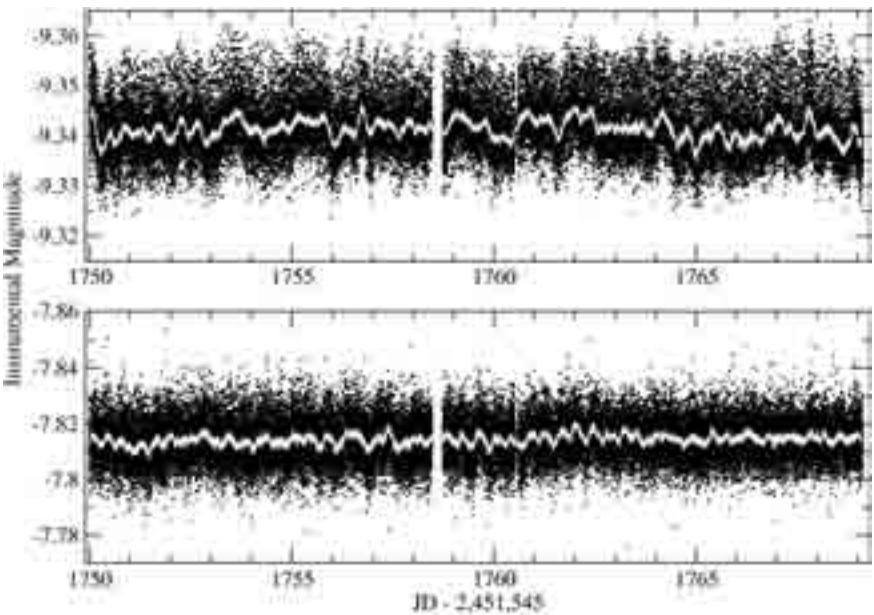

Figure 12: Final light curves of g0 (HD 20884, upper panel) and g1 (HD 20790, lower panel). Moving averages over 200 data points are overplotted.

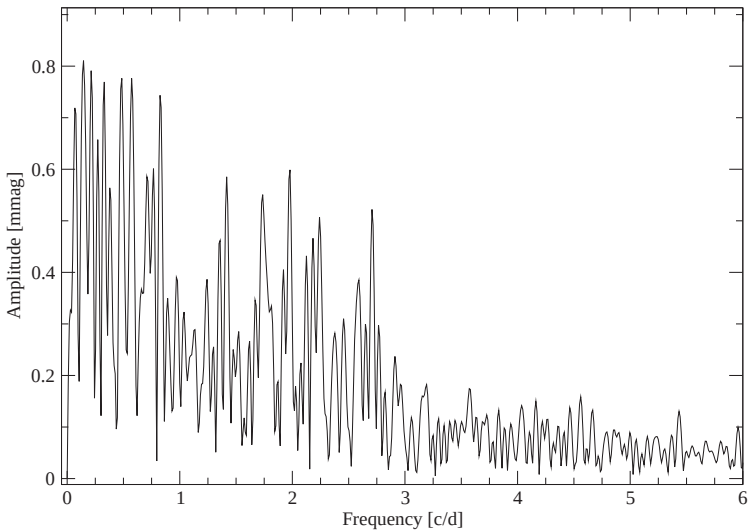

Figure 13: Fourier spectrum of HD 20884.

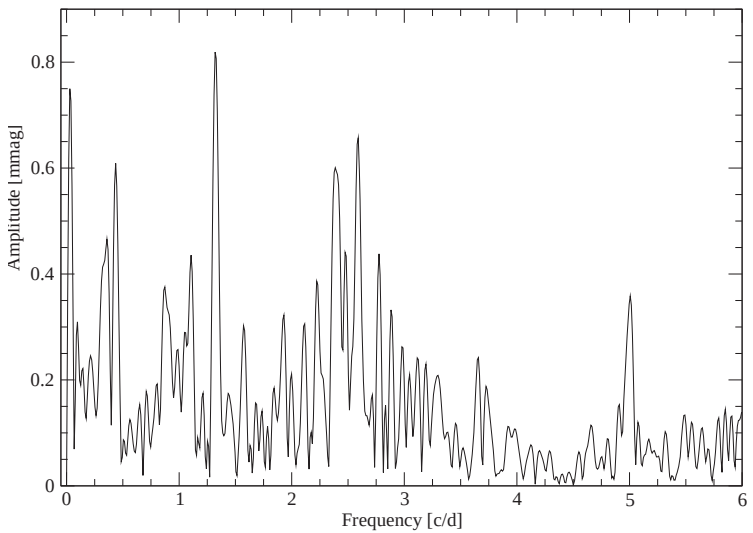

Figure 14: Fourier spectrum of HD 20790 (Guide Star g1 of the κ^1 Ceti run 2004).

The γ Dor star HD 20790

Fig. 14 shows the amplitude spectrum of this star. The significant intrinsic frequencies identified after frequency analysis and comparison to g2 and g3 are listed in Table 4. We adopt the frequency error estimation from Kallinger et al. (2008b) for the case of closely spaced frequencies, which yields an uncertainty of 0.013 d^{-1}. The observed frequency range is typical for γ Dor pulsators. Two frequencies, f_3 and f_4, are spaced by 1 d^{-1}. Due to the clean spectral window (see Fig. 10), rather than due to aliasing, we consider these frequencies intrinsic.

In November 2004 classification spectra were taken by one of us (SR) taken at David Dunlap Observatory (DDO), using the Cassegrain spectrograph on the 1.88 m telescope. See Kallinger et al. (2008a) for the classification of all four Guide Stars of this run. The spectral classification for HD 20790 resulted in a spectral type of F4IV and a rough $v \sin i$ estimate between 80 and 130 kms^{-1}. The quality of our classification spectrum does not allow us to achieve a more precise determination of $v \sin i$. Nevertheless, we may consider this star a fast rotator.

The Strømgren calibration using the software TempLogG (Kaiser 2006) and the measurements published by Hauck & Mermillod (1998) lead to $T_{\mathrm{eff}} \approx 7000$ K, log g $\approx$ 3.8 and [Fe/H] $\approx$ 0.04. These values place HD 20790 in the γ Dor instability strip.

The new HIPPARCOS parallax (Leeuwen 2007) of HD 20790 is 6.7$\pm$0.86 mas, and the apparent magnitude given in SIMBAD is $V = 8.9$. The calculation of M_V and $L/L_\odot$ was performed as for HD 20884 above. The bolometric correction for early F type stars is about zero and neglected, as well as the extinction, due to the small distance. We find a luminosity range between 3.8 and 6.4 $L_\odot$, which is compatible with γ Dor stars.

Label	Frequency $[\mathrm{d}^{-1}]$	Significance	Amplitude [mmag]
f_1	0.88	11.4	0.34
f_2	1.32	57.3	0.87
f_3	1.39	5.9	0.27
f_4	2.39	28.0	0.59
f_5	2.42	14.8	0.42
f_6	2.47	19.4	0.51
f_7	2.59	36.9	0.62
f_8	2.77	18.5	0.46

Table 4: Frequencies identified in HD 20790.

Analysis of the Guide Stars from the HR 1217 Run

The light curves show strong instrumental artifacts between JDM 1777 and 1790 not caused by the Moon, since the angular separation in this time interval was at its maximum. These artifacts introduce power at low frequencies into the Fourier spectrum. Additionally, there are a major gap of 0.9 d between JDM 1783.4 and 1784.3 as well as some minor gaps due to software crashes on-board the spacecraft. The data reduction was performed using the decorrelation method. The RMS deviation of the data sets for g1 and g2 decreased by 23.5% and only 2.2%, respectively. Although the RMS error is reduced, the point-to-point scatter is increased for g1.

Fig. 15 illustrates the effect of decorrelation for g1. The raw light curve (bottom) shows periodic spikes due to overcorrection of the background in the on-board reduction. Clipping the outliers removes these spikes, whose periodicity is the MOST orbit frequency. Due to the periodic clipping of outliers, peaks at the MOST orbit frequency and harmonics arise in the spectral window (see Fig. 16). Nevertheless, the aliasing effect does not cause significant problems to the frequency analysis, because the amplitudes in the spectral window are modest.

Fig. 17 compares three reduced light curves of stars with similar brightness (g0, g1 and g6). These stars show similar light curves and artifacts in the middle of the observations, hence they are well-suited as direct comparison stars after the data reduction. The overplotted moving medians over 300 datapoints (3.26 h) do not show periodicities for g0 and g6, while the moving median of g1 (HD 24217) displays the intrinsic pulsation including beating. The artifacts cause low-frequency power in the Fourier spectrum with similar amplitudes in the three stars, hence the instrumental signal can be identified and distinguished from stellar signal.

ID	GSC-ID	HD / BD	SpT.	V [mag]	parallax [mas]
g0	05307-00865	HD 24134	F2V	8.94	8.23 ±1.00
g1	05307-00953	HD 24217	A2m	9.23	-
g2	05307-01032	HD 24338	M2III	7.35	4.24 ±0.75
g3	05307-01312	BD -12 739	-	10.14	-
g4	05307-01021	HD 24183	F6V	7.75	13.41 ±0.61
g5	05307-01261	BD -12 738	-	9.86	-
g6	05307-00817	HD 24172	F6/F7V	9.25	-

Table 5: Information on the Guide Stars in the HR 1217 field, taken from the SIMBAD data base. The parallaxes available for three stars are taken from the new HIPPARCOS Catalogue (van Leeuwen 2007).

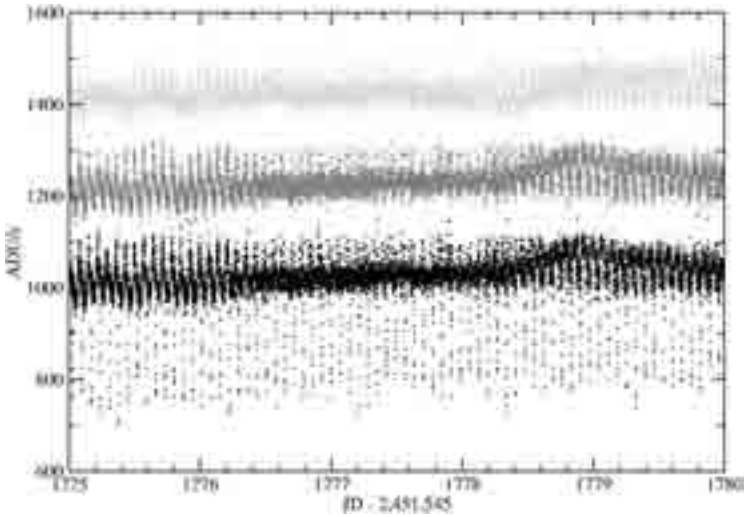

Figure 15: Effects of decorrelation on the g1 data. The light curve in the middle represents the result of a 3-σ clipping using a moving average on the raw data (bottom). The decorrelated data are displayed on top. In this plot 5 days of observation are presented for better visibility. Vertical offsets of the three plots are arbitrary.

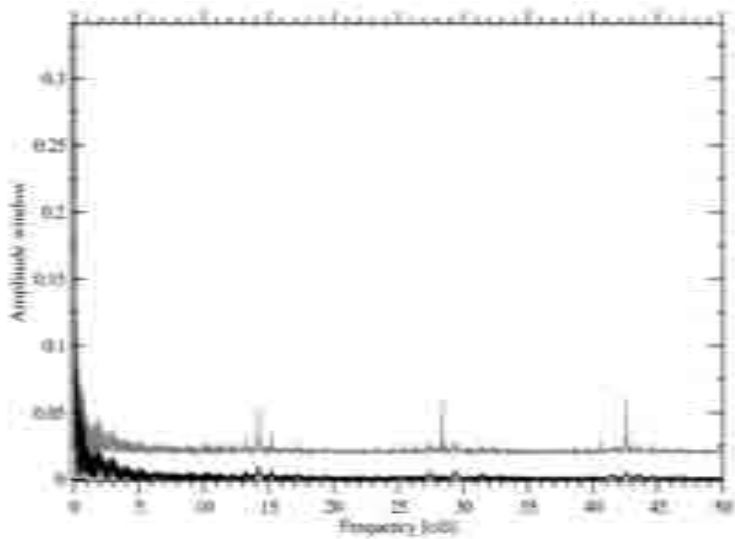

Figure 16: Comparison of the spectral windows for the raw data (black line) and the processed data (red line, offset 0.02 vertically for better visibility) for the HR 1217 field. Aliasing in the reduced Guide Star time series is modest, however present.

ID	Standard deviation [mmag]	Point-to-point scatter [mmag]
g1 raw	27.052	11.990
g1 reduced	20.691	12.520
g2 raw	66.345	15.913
g2 reduced	64.917	15.482

Table 6: Change in standard deviation and point-to-point scatter of the two variables among the HR 1217 Guide Stars. Even though the standard deviation decreases after data reduction, the point-to-point scatter increases.

Label	Frequency [d^{-1}]	Significance	Amplitude [mmag]
f_1	2.138	62.3	1.86
f_2	2.265	132	2.86
f_3	2.404	69.6	1.93
f_4	2.577	20.4	1.03

Table 7: Identified frequencies of HD 24217.

Results of the Guide Stars from the HR 1217 Run

HD 24217

The second variable star HD 24217 (g1) is an A2m star, according to SIMBAD. The HD Catalogue classifies it as F0, whereas the Michigan Catalogue of two-dimensional spectral types for HD stars (Vol. 4) gives A2mA7-F2/3 (Houk & Smith-Moore 1998). The star shows signal in the lower frequency range around 2.26 d^{-1}, which is typical for γ Dor stars. The star g0 (HD 24134) was used as a direct comparison to identify possible instrumental effects. HD 24134 is classified as F2V and may be also a γ Dor star. However, no significant variability was detected. Fig. 18 displays the Fourier spectra of both stars overplotted. HD 24217 shows four frequencies in the range of 2.1 to 2.6 d^{-1}. In the lower frequency range, the amplitude spectra are nearly identical. We consider the low amplitude peaks in the range of 15 to about 20 d^{-1} to be due aliasing rather than to intrinsic p-mode pulsation. The identified frequencies are given in Table 7, and the uncertainties of the frequencies are estimated to 0.009 d^{-1}.

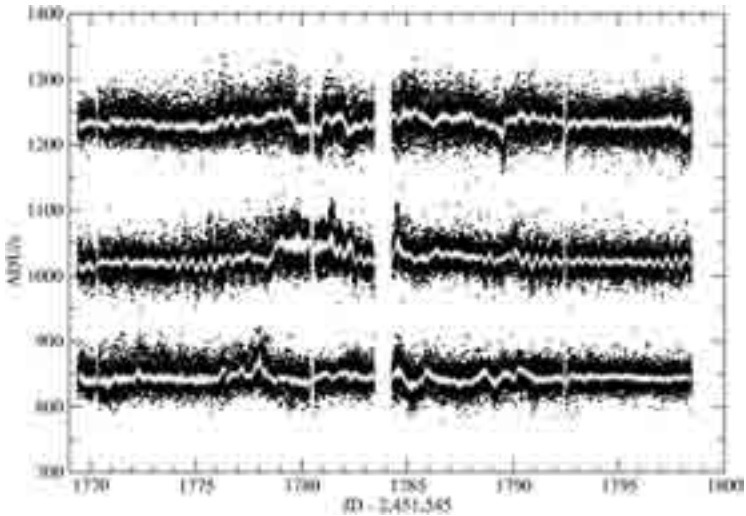

Figure 17: Reduced light curves of g0 (top), g1 (HD 24217, middle) and g6 (bottom) with a moving median over 300 datapoints (3.26 h) overplotted. These three Guide Stars are of similar brightness and show artifacts in the middle of the observing run.

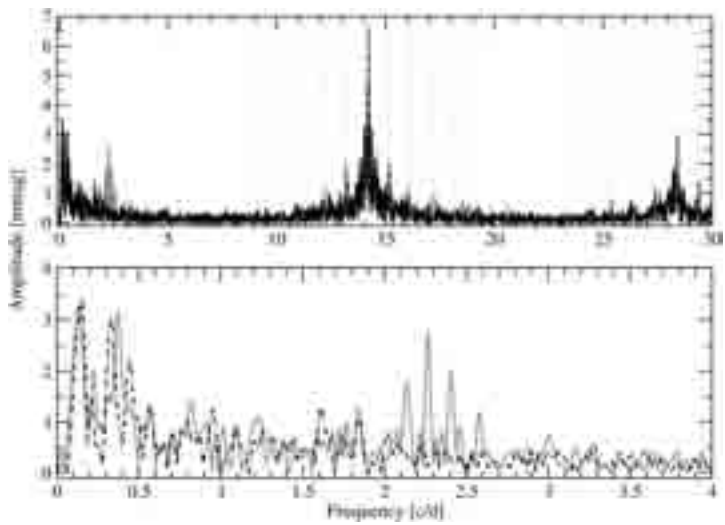

Figure 18: Fourier amplitude spectra for HD 24217 and the comparison star HD 24134. The frequency range from 0 to 30 d^{-1} is shown in the top panel, the range from 0 to 4 d^{-1} in the bottom panel. The dashed-dotted line (bottom panel) corresponds to the Fourier transform of the comparison star. The dashed-dotted vertical lines in the top panel indicate the MOST orbit frequency, its first harmonic, and 1 d^{-1} side lobes.

HD 24338

HD 24338 is listed in the Combined General Catalogue of Variable Stars (CGCVS, Samus et al. 2004), but no further information on its variability could be found in the literature. The light curve of HD 24338 is shown in Fig. 19. To determine the period of the long-term variability, Phase Dispersion Minimization (PDM) was applied, displayed by Fig. 20. The lowest error was obtained at a period of 17.38 d. There is a secondary minimum at 8.8 d which is due to the less pronounced secondary minimum in the light curve.

The uncertainty in the period determination is estimated to ± 0.2 d. The amplitude of the 17.4 d variation is about 40 mmag. The observed variations may well be due to large starspots and the period of 17.4 d corresponds to the rotation period of the star, based on the assumption that both deep minima in the light curves are caused by the same star spot. We also note that we only observe less than twice this variation cycle and that the second deep minimum could be caused by another spot. To derive more reliable conclusions, longer time base observations are required.

Discussion and Conclusions

A data reduction pipeline for MOST Guide Star photometry based on the decorrelation technique is presented. The pipeline consists of two IDL programs, one for data extraction and one for data reduction. Since MOST observes at least four Guide Stars in one field simultaneously, common instrumental signal can be identified and mitigated, in some cases even by a factor of 10. If appropriate comparison stars are available, three-star photometry, which is common for ground based observations, can be applied. However, in many cases comparison stars are much too faint or are affected quite differently by stray light. The decorrelation method can deal with these conditions in a much better way.

The number of decorrelation steps is crucial for the method discussed here. If many non-variable Guide Stars are available, many decorrelation steps can be performed, which results in good final light curves shown in Fig. 3. To the contrary, if only a few reference stars are available, the results may not be significantly better than the raw light curves after outlier clipping, especially if the comparison stars are rather faint, like in the presented case of κ^1 Ceti 2004 Guide Stars. However, a considerable reduction of the time series' variance can be achieved, if the variable and the comparison stars are similar in brightness.

Data smoothing techniques, which are applied to Guide Stars individually, have the disadvantage that the information provided by other stars is ignored. Bandpass filters, for example periodic filter functions, may strongly decrease the stellar signal at frequencies close to the instrumental frequencies, which makes the filter techniques unsuited for data variables with low-frequency signal like γ Dor stars or signal in the vicinity of the MOST artifacts like δ Scuti stars.

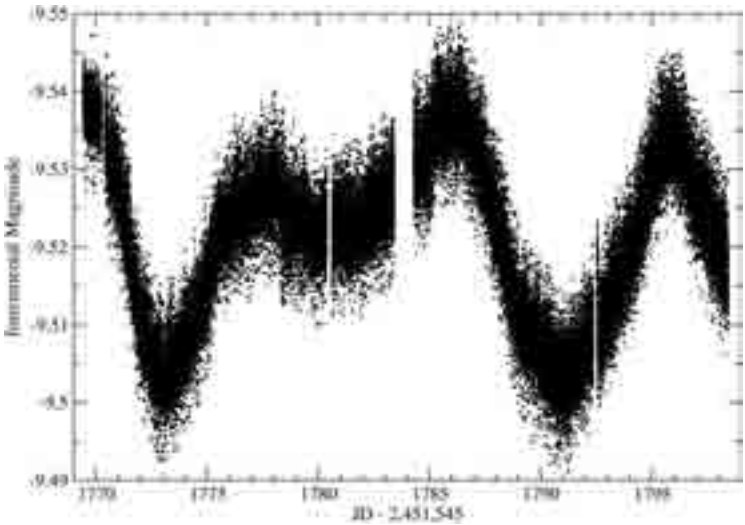

Figure 19: Light curve of HD 24338, an M2III star.

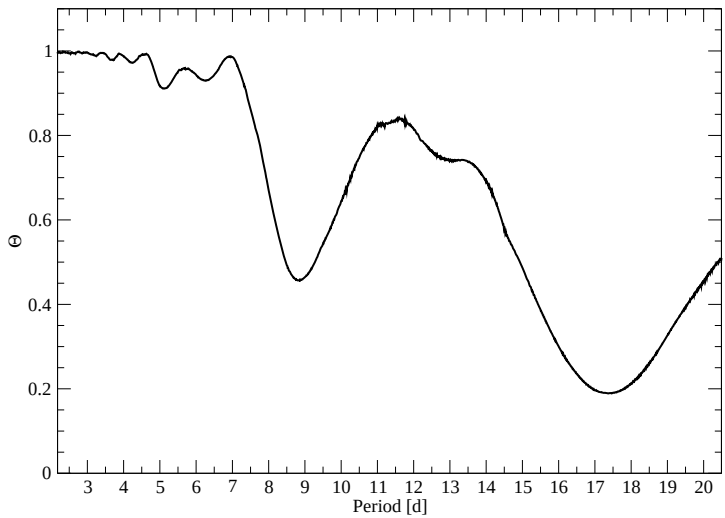

Figure 20: PDM method applied to the light curve of HD 24338. The minimum of the error is at about 17.38 days, and a secondary minimum is present at 8.83 d.

The MOST Guide Star photometry presented here contains four variables: (1) one pulsating K giant (HD 20884) and (2) one M giant most probably showing large starspots. Assuming that the first and the second deep minimum in the light curve of the M giant is due to the same spot, the rotation period of this star would be about 17.4 d. Additionally, we report on two new γ Dor star discoveries, (3) HD 20790 and (4) HD 24217. Our classification spectrum and the published Strømgren colors justify the γ Dor classification for HD 20790, while no published Strømgren colors and no classification spectrum for HD 24217 are available. Moreover the spectral classification in the literature, especially the classification in the Michigan Catalogue A2mA7-F2/3 indicates chemical peculiarities of this star. A few high-resolution spectra for abundance analysis could help to clarify this situation and the possible binarity.

Acknowledgments. MH and WW are supported by the Austrian Fonds zur Förderung der wissenschaftlichen Forschung (FWF, project *The Core of the HR diagram*, P 17580-N02) and the Bundesministerium für Verkehr, Innovation und Technologie (BM.VIT) via the Austrian Agentur für Luft- und Raumfahrt (FFG-ALR). JMM, SR, DBG, and AFJM received research support from NSERC (Natural Sciences & Engineering Research Council) Canada. RK was partly funded by the Canadian Space Agency. DS is supported by the National Science Foundation.

References

ESA 1997, *The Hipparcos and Tycho Catalogues*, ESA-SP 1200

Hauck, B., Mermillod, M. 1998, A&AS, 129, 431

Houk, & Smith-Moore 1998, Michigan Catalogue of HD stars Vol. 4

Huber, D., & Reegen, P. 2008, CoAst, 152, 77

Kaiser, A. 2006, ASPC, 349, 257

Kallinger, T., Guenther, D. B., Weiss, W. W., et al. 2008a, CoAst, 153, 84

Kallinger, T., Reegen, P., & Weiss, W. W. 2008b, A&A, 481, 571

Matthews, J. M., Kuschnig, R., Guenther, D. B., et al. 2004, Nature, 430, 51

Reegen, P., Kallinger, T., Frast, D., et al. 2006, MNRAS, 367, 1417

Reegen, P. 2007, A&A, 467, 1353

Rowe, J. F., Matthews, J. M., Kuschnig, R., et al. 2006, MmSAI, 77, 282

Rucinski, S. M., Walker, G. A. H., Matthews, J. M., et al. 2004, PASP, 116, 1093

Samus, N. N., Durlevich, O. V., et al. 2004, Combined General Catalogue of Variable Stars

van Leeuwen, F. 2007, A&A, 474, 653

Walker, G. A. H., Matthews, J. M., Kuschnig, R., et al. 2003, PSAP, 115, 1023